J. Webster (ed.), *Wiley Encyclopedia of Electrical and Electronics Engineering*

PROPAGATION AT EXTREMELY LOW FREQUENCIES

Extremely low frequency (*ELF*) electromagnetic waves (frequencies in the range 3 Hz to 3 kHz) are of interest in the sciences and in communications for a number of reasons. Perhaps most important, lightning is a powerful natural source of electromagnetic radiation in this frequency range, and the characteristics of lightning can be studied in considerable detail by making measurements on the waves it generates. In a communications context, the naturally occurring lightning-generated waves constitute a noise background that can degrade an ELF communications link. On the other hand, ELF waves travel with little attenuation to large distances in the space between the earth's surface and the ionized upper layers of the earth's atmosphere (i.e., the ionosphere), and thus they can provide communications over large regions of the earth. Furthermore, compared with the other, higher-frequency forms of electromagnetic waves used for communications, ELF waves are largely unaffected by disturbances in the ionosphere, and thus they can provide a more reliable communications link during times of high solar activity. Finally, they penetrate quite well through the conducting materials typically encountered on the earth's surface, and thus they can be used for probing the surface, for prospecting, and for certain forms of communication through the earth and the sea.

In this article, we provide a brief description of the propagation characteristics of these waves based on a simplified model of ELF electromagnetic wave propagation in the earth–ionosphere waveguide. We discuss some interesting consequences of the long-distance propagation of ELF waves through the waveguide, one of which is the focusing of the waves at the antipode of the source. Another is the occurrence of resonance in the waveguide. We also discuss some practical applications of ELF waves and the special considerations that can affect communication systems.

In order to better understand ELF wave propagation in the earth–ionosphere waveguide, the electrical properties of the waveguide walls need to be taken into account, as well as the effect of dynamic changes in the ionosphere. Another factor affecting the waveguide is the geomagnetic field, which causes the waveguide to be anisotropic. Finally, because the complexity of the waveguide makes its analytical description difficult, we discuss the two most common methods for calculating the solution to particular ELF wave propagation problems.

Simplified Waveguide Model

A simple approximation of the earth–ionosphere waveguide, which is nonetheless useful in many situations, is the flat earth model. The waveguide is modeled as an infinite parallel-plate waveguide with the curvature of the earth and the ionosphere neglected. Figure 1 presents the geometry with a cylindrical coordinate system (ρ, ϕ, z). The ground plane is located at $z = 0$, and the ionospheric boundary is at $z = h$.

This model is valid only for distances of up to half an earth radius from the source, because at greater distances the curvature of the earth affects ELF propagation.

The walls of the waveguide are modeled as perfect conductors, because in the ELF range both the earth and the ionosphere have very high conductivities.

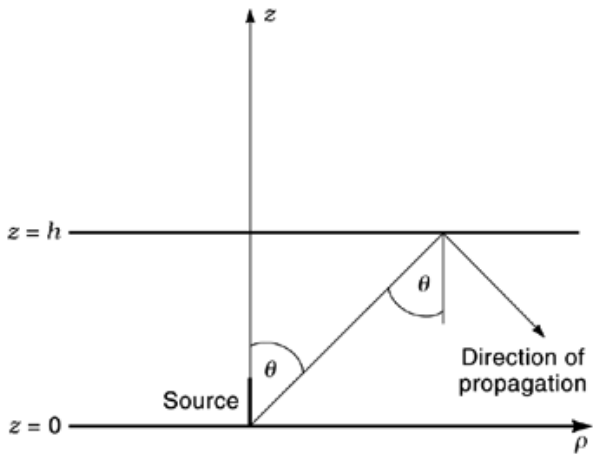

Fig. 1. Geometry of the flat-earth–ionosphere waveguide with a cylindrical coordinate system.

The vertical component of the electric field generated by a vertical electric dipole of moment Ids, placed on the ground at the point ($\rho = 0, z = 0$) in a flat waveguide with perfectly conducting walls, is described by Wait (1) as a modal series:

$$E_z = E_0 \frac{(\rho/\lambda)^{1/2}}{(h/\lambda)} e^{j(k\rho - \pi/4)} \sum_{n=0}^{\infty} \delta_n S_n^{3/2} e^{-jKS_n\rho} \cos(kC_n z) \qquad (1)$$

where

λ = free-space wavelength

$k = 2\pi/\lambda$

$\eta = \sqrt{\mu_0/\epsilon_0} \approx 120\pi\ \Omega$ is the free-space impedance

$E_0 = -i(\eta Ids/\lambda)\, e^{-jk\rho}/\rho$

$$\delta_n = \begin{cases} \frac{1}{2}, & n = 0 \\ 1, & n = 1, 2, \ldots \end{cases}$$

$= S_n \sin\theta_n \sqrt{1 - C_n^{1/2}}$ sine of the eigenangle of the nth mode (which may be complex)

$C_n = \cos\theta_n$ cosine of the eigenangle of the nth mode

θ_n = eigenangle of the nth mode.

Equation (1) describes the field measured within the waveguide, for $0 < z < h$. It is a far-field approximation, valid at big enough distances from the source ($h \ll \rho$ and $\lambda \ll \rho$), where $\rho > 300$ km can be taken as a lower limit. See Bannister (2) for a development of field expressions at shorter distances from the source. The time dependence is $e^{j\omega t}$, where $\omega = 2\pi c/\lambda$ is the angular frequency.

The other field components, in addition to E_z [Eq. (1)], can be calculated using Maxwell's equations, and they are described by

$$H_\phi = \frac{E_0}{\eta} \frac{(\rho/\lambda)^{1/2}}{(h/\lambda)} e^{j(k\rho - \pi/4)} \sum_{n=0}^{\infty} \delta_n S_n^{1/2} e^{-jkS_n\rho} \cos(kC_n z) \qquad (2)$$

$$E_\rho = E_\phi = H_z = H_\rho = 0 \qquad (3)$$

The modal phase velocity is $c/\mathrm{Re}[S_n]$, and the modal attenuation factor is $-k$ Im $[S_n]$ per unit distance.

The eigenangle θ_n can be interpreted as the incidence angle of the wavefront on the ionosphere, as indicated in Fig. 1. This interpretation of the eigenangle is closely related to the ray-theory description of electromagnetic wave propagation in the waveguide, which is an alternative to the modal theory discussed here. However, the ray-theory treatment of the waveguide is of little consequence in the ELF band, so it is not discussed further.

The modes generated by the vertical dipole are all transverse magnetic (TM) modes, since the magnetic field is transverse to the direction of propagation of the wave as it propagates away from the source (and thus $H_\rho = 0$).

Nickolaenko and Hayakawa (3) calculate the spectrum in the ELF band of the vertical electric field generated by a vertical dipole, from expressions based on the modal series, and demonstrate the Schumann resonance, a phenomenon that will shortly be described.

A horizontal electric dipole source of moment Ids, placed at ($z = z_0$, $\rho = 0$) parallel to the $\phi = 0$ direction, generates a magnetic field whose vertical component is

$$H_z = -\frac{\sin\phi}{\eta} E_0 \frac{(\rho/\lambda)^{1/2}}{(h/\lambda)} \frac{e^{j(k\rho-\pi/4)}}{2} \sum_{m=1}^{\infty} S_m^{1/2} \sin(kC_m z_0) \sin(kC_m z) e^{-jkS_m\rho} \qquad (4)$$

where

S_m = $\sin\theta_m$

$\sqrt{1-C_m^2}$ = sine of the eigenangle of the mth mode.

C_m = cos

θ_m = cosine of the eigenangle of the mth mode

θ_m = eigenangle of the mth mode

Equation (4) is an approximation valid for $0 \le z < h$, $h \ll \rho$, and $\lambda \ll \rho$, where $\rho > 300$ km can be taken as a lower limit for its validity. The time dependence is $e^{j\omega t}$. The other components of the field are zero, except for E_ϕ and E_r.

The modes generated by the horizontal dipole in the broadside direction are transverse electric (TE) modes, since the electric field is transverse to the direction of propagation of the wave (and thus $E_\rho = 0$). In other directions, the horizontal dipole generates a mixture of TM and TE modes. The TE waves are weak at low altitudes (near the ground), because the horizontal electric field is extinguished near the conductive earth. Since most measurements of ELF fields are made by antennas mounted on the ground, the TE component they receive is weak. This is possibly the reason that the TE modes receive little attention in the scientific literature.

The modal equations (5) and (6) of the simple flat earth model with perfectly conducting walls determine the eigenangles of the waveguide:

$$e^{-j2khC_n} = e^{-j2\pi n} \qquad n = 0, 1, 2, \ldots \qquad (5)$$

$$e^{-j2khC_m} = e^{-j2\pi m} \qquad m = 1, 2, \ldots \qquad (6)$$

for the TM and TE modes respectively.

The eigenangles for the TM mode are

$$C_n = n\frac{\lambda}{2h}, \qquad n = 0, 1, \ldots \qquad (7)$$

and for the TE modes are

$$C_m = m\frac{\lambda}{2h}, \qquad m = 1, 2, \ldots \tag{8}$$

The lowest TM mode is the 0th, which propagates over the whole frequency range. This mode is also called the *transverse electromagnetic* (TEM) mode, because both the electric and the magnetic fields are transverse to the direction of propagation. The electric field is vertical (E_z component only), and the magnetic field is in the ϕ direction.

The higher modes, namely the TM modes with $n = 1, 2, \ldots$ and all the TE modes, propagate above a certain frequency, called the cutoff frequency, which characterizes each mode. The cutoff frequency of high-order modes is higher than that of the lower-order modes. Only the first mode is of interest in the ELF range, because the cutoff frequencies for all the higher modes are above 3 kHz. The cutoff frequency of these first modes (TM and TE) varies between 1.5 kHz and 4 kHz, depending on the height of the ionosphere.

When extending the waveguide model from the simple flat, perfectly conducting plate model, the following features may be considered:

- The reflections coefficients of the earth and the ionosphere
- The waveguide geometry
- The presence of the geomagnetic static field

The effects of these features of the waveguide on the ELF waves propagating within it are discussed in the section "Extensions of the Waveguide Model" below.

Applications

ELF waves propagating in the earth–ionosphere waveguide undergo very low attenuation (sometimes as low as 1 dB/Mm to 2 dB/Mm). This allows ELF transmissions to propagate great distances, making this frequency range suitable for communication networks encompassing the whole globe. Bannister (4) discusses the attenuation in the ELF band and shows measurements of the attenuation rate at different frequencies.

Another important feature of ELF waves is their good penetration into the earth and sea water. The skin depth, which characterizes penetration of electromagnetic waves into lossy materials, varies inversely as the square root of the wave frequency ($\delta \propto 1/\sqrt{\omega}$). Thus, ELF waves have a larger skin depth than waves in higher frequency bands, and they penetrate better into conducting materials. For example, the skin depth of waves propagating at 70 Hz in sea water is 30.1 m. The large skin depth is the reason for operating submarine communication systems in the ELF range. An example of such a system is the United States Navy's ELF Communications System for communication with submarines, operating in the frequency range of 70 Hz to 80 Hz. This system consists of two synchronous transmitters connected to 22.5 km quasi orthogonal antennas.

The major difficulties when communicating in the ELF range are the need for large antennas and the low data rate. In order to achieve efficient transmission, the physical dimensions of the antennas should be comparable to the wavelength of the communication frequency, so the long wavelengths inherent in the ELF range (100 km at 3 kHz up to 100,000 km at 3 Hz) make efficient antenna installation very difficult. This is a problem mainly in the transmitters, since on the receiving side the antenna preamplifier combination is limited only by atmospheric noise in the frequency range of interest.

The useful bandwidth in an ELF communication system is limited by the low carrier frequency. Communication systems in the ELF range typically transmit at very low data rates compared to systems utilizing other frequency bands.

The large antenna dimensions needed for efficient transmission and the inherent low bandwidth are the reasons that ELF communication systems are few and are usually run by governments for limited military usage.

Kelly (5) surveys engineering issues related to ELF systems, namely modulation, dispersion, antenna and system performance, and coverage predictions.

Electrojet Modulation. One scientific application in the ELF band is the modulation of ionospheric currents, in particular the auroral electrojet. The auroral electrojet is an intense westward current, flowing in the D and E regions of the ionosphere (the section "Ionospheric Reflection" below discusses the ionospheric layers). It flows within the auroral belt, a narrow oval-shaped region encircling the north geomagnetic pole (a similar belt exists around the south pole).

The intensity of the auroral electrojet is affected by the conductivity of the ionospheric D and E layers. Changes in the ionospheric conductivity can be induced artificially by heating the ionosphere with radio waves of appropriate frequency in the HF band, which are efficiently absorbed in the D and E layers. Amplitude-modulated heating of the D and E layers translates into amplitude-modulated conductivity of the medium, which modulates the intensity of the electrojet. The modulated electrojet reradiates into the earth–ionosphere waveguide at the modulation frequency. Villaseñor et al. (6) study different modulation methods and polarizations of the heating wave, and Barr and Stubbe (7) discuss the radiation mechanism and evaluate the intensity of the radiated wave. Papadopoulos et al. (8) discuss the efficiency of the ELF/VLF generation process.

Generation of ELF/VLF signals by modulation of the auroral electrojet has been demonstrated in various *ionospheric heating* facilities. Experiments of this kind are discussed by Stubbe et al. (9), Ferraro et al. (10), Barr et al. (11), Rietveld at el. (12), and Barr et al. (13).

Background Noise

The sources of noise in the ELF range are lightning discharges, man-made noise, and magnetospheric phenomena (such as chorus and hiss); among these, lightning discharges and man-made noise dominate. The low attenuation in this band allows the signals generated by lightning strokes, called atmospherics, or *sferics*, to travel great distances around the earth. Thus, a lightning discharge above Africa can be easily detected by a receiver in North America. It is estimated that on average there are roughly 2000 thunderstorms active around the earth at any moment, generating an average of 100 to 200 lightning strokes per second. This lightning activity constitutes the major source of noise in the ELF range. Power-line harmonics are a major source of man-made noise in the ELF, and their effect is evident throughout the whole frequency band in inhabited areas.

The background power spectrum in the ELF range is generally of the form $1/f^{\alpha}$ [Galejs (14), Chap. 7], where α is typically close to 2. Maxwell (15) and Maxwell and Stone (16) show measurements of the background noise level at various location, and in (15) they discuss the dependence of the background noise spectrum on latitude. It is shown that the noise spectra correlate well with lightning spectra and propagation attenuation coefficients. The background noise varies with a period of 24 h because of diurnal variations of global thunderstorm activity, and the seasonal variation of the noise is related to global thunderstorm activity. Gustafsson et al. (17) and Smith and Jenkins (18) present background-level measurements recorded in northern latitudes, and demonstrate that the daytime background level is generally lower than the nighttime level. They suggest that the reason is enhanced ionospheric absorption during the day.

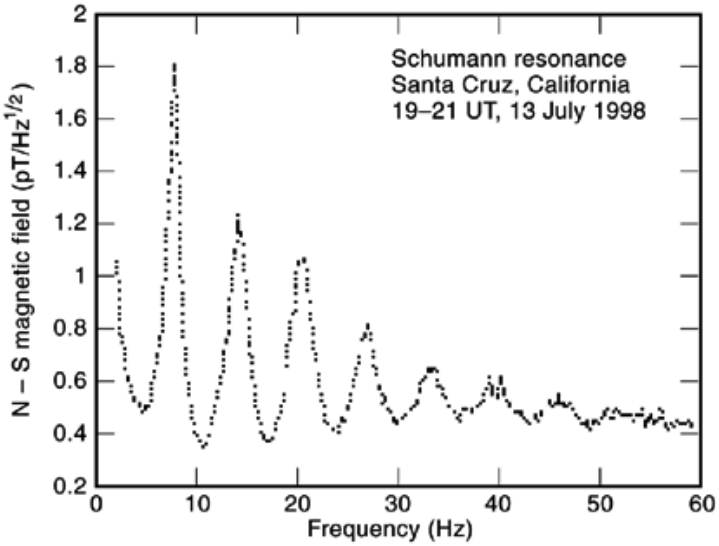

Fig. 2. Spectrum of the first eight Schumann resonance modes. The basic resonance mode occurs when the wavelength approximately equals the circumference of the earth.

The Schumann Resonance

An interesting phenomenon in the lower end of the ELF band is the Schumann resonance, named after W. O. Schumann, who predicted it in 1952. The basic resonance mode (frequency 7.5 Hz) occurs when the wavelength of the propagating wave approximately equals the circumference of the earth (40,000 km). Constructive interference at the basic Schumann resonance and its harmonics results in an increased background noise level at these frequencies (Fig. 2).

Derivations of the Schumann resonance from general field expressions are presented by Wait (19) and Jones (20), and extended by Large and Wait (21) to include the effects of the day–night inhomogeneity of the ionosphere. The Schumann resonance was first observed in 1960 by Balser and Wagner (22).

It is thought that the main source of energy for the Schumann resonance is lightning strokes occurring around the earth, and that, as a result, the resonance level is an indication of global lightning activity [Balser and Wagner (23), Nickolaenko et al. (24,25), Ogawa et al. (26), and Heckman et al. (27)]. The Schumann resonance is used to locate thunderstorms [Polk (28) and Galejs (29)] and to study the ionosphere [Sentman and Fraser (30)]. Sao et al. (31) relate diurnal variations of the Schumann resonance frequency to solar ionizing radiation, solar zenith angle, and geomagnetic disturbances.

The interest in the Schumann resonance was revived in the 1990s, when Williams (32) showed a correlation between the intensity of the first mode of the Schumann resonance and the fluctuations of the temperature in the tropical atmosphere. This suggests that the Schumann resonance can be used to monitor global climate changes. A recent summary on the Schumann resonance with many references is found in Nickolaenko (33).

Extension of The Waveguide Model

The modal theory of the earth–ionosphere waveguide is extended in this section from the simplified parallel-plate model with perfectly conducting walls, which was presented in the section “Simplified Waveguide Model.”

The extensions of the waveguide model presented here are:

- Consideration of the electrical properties of the earth and ionosphere and calculation of the reflection coefficients of the waveguide walls
- Consideration of the spherical geometry of the earth, which imposes a spherical waveguide instead of a planar one
- Consideration of the geomagnetic field, which causes anisotropic ionospheric reflections.

Reflection Coefficients. An accurate model of the earth–ionosphere waveguide for ELF wave propagation has to take into account the finite conductivities of the two limiting boundaries. The conductivity of the earth ranges from 10^{-4} S/m for dry rocky areas to 4 S/m for sea water, and the dielectric constant varies considerably as well. A list of the conductivity and the dielectric constant values of various types of soil and water is included in Ref. 34. The earth is usually treated as a uniform sharp boundary, even though this model does not strictly apply to its changeable surface. The validity of the smooth earth model stems from the small scale of change of the surface compared to the long wavelengths involved in ELF propagation.

A further extension of the waveguide should take into account the inhomogeneity of the earth's surface conductivity. This extension of the waveguide theory is similar in nature to the theory related to ionospheric inhomogeneities discussed in the section "The Inhomogeneous Ionosphere" below.

A realistic model of the ionosphere is more involved, since it depends on the concentration of free electrons and various positive ions, which in turn depend on complex generation mechanisms. The section "Ionospheric Reflection" below discusses the calculation of ionospheric reflection coefficients in more detail.

Another complication of the calculation of the ionospheric reflection coefficients stems from the fact that the ionospheric boundary is not sharp. In many cases, an effective height is calculated for the waveguide model, and reflection is treated as though the ionosphere were sharply bounded at this height. Booker and Lefeuvre (35) calculate the effective ionospheric height for a simple profile of ionospheric ionization density, and show that it is frequency-dependent. Greifinger and Greifinger (36) present a more complicated reflection model, which includes two ionospheric reflection layers at different heights.

The reflection coefficients of the earth and the ionosphere affect the eigenangles of the different modes. These in turn determine the attenuation that each mode undergoes and the relative amplitudes of the modes. The relation between the eigenangles of the different modes and the attenuation can be appreciated by noting that if S_n is complex in Equations (1), (2), and (4), then its imaginary part translates into attenuation through the exponential factor $e^{-jkSn\rho}$. The effect of the reflection coefficients on the eigenangle can be appreciated by looking at the modal equation, shown here for the TM modes:

$$R_{\mathrm{i}}(\omega, \theta_n) R_{\mathrm{e}}(\omega, \theta_n) e^{-j2kh(\omega)C_n} = e^{-j2\pi n}, \qquad n = 0, 1, 2, \ldots \tag{9}$$

where $R_{\mathrm{i}}()$ is the ionospheric reflection coefficient for TM waves, $R_{\mathrm{e}}()$ is the earth reflection coefficient for TM waves, and $h(\omega)$ is the frequency-dependent effective reflection height. Both reflection coefficients depend on the frequency ω and on the eigenangle θ_n.

Waveguide Geometry. The waveguide geometry affects the various modes [Eqs. (1) and (4)]. It has a minor effect on the modal equation (9), so the eigenangles are not strongly affected by the flat-earth simplification.

When considering a spherical geometry rather than a parallel-plate geometry, mode coupling is introduced. This means that TM waves propagating in the waveguide are partially converted to TE waves because of reflections from the curved walls of the waveguide (and likewise TE waves are converted to TM).

Expressions for the fields in a spherical waveguide are given by Wait (1), using a spherical coordinate system (r, θ, ϕ). The earth is modeled as a homogeneous sphere of radius a (= 6370 km), conductivity, σ_{g}, and

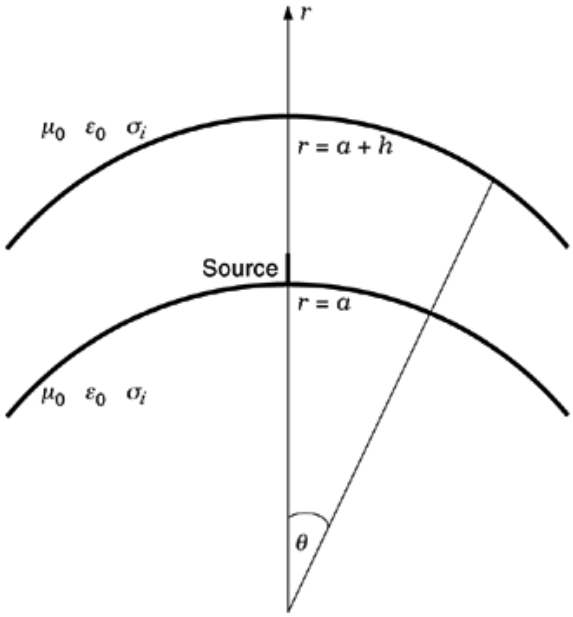

Fig. 3. Geometry of the spherical earth–ionosphere waveguide with a spherical coordinate system.

dielectric constant ϵ_g. The lower edge of the ionosphere is located at $r = a + h$, its conductivity is σ_i, and its dielectric constant is ϵ_i. It is assumed that both the earth and the ionosphere are good but not necessarily perfect conductors. The source is a vertical electric dipole located at ground level at $r = a$, $\theta = 0$, $\phi = 0$, and the observation point is located on the ground at $r = a$, θ, $\phi = 0$ as in Fig. 3.

The vertical electric field in this configuration is

$$E_r = E_0 \left(\frac{d/a}{\sin(d/a)} \right)^{1/2} \frac{(d/\lambda)^{1/2}}{(h/\lambda)} e^{j[2\pi(d/\lambda)-\pi/4]} \sum_{n=0}^{\infty} \delta_n S_n^{3/2} e^{-j2\pi S_n(d/\lambda)} \tag{10}$$

where

λ = free-space wavelength
$d = a\theta =$ arc length between the source and the observer
$\eta = \sqrt{\mu_0/\epsilon_0} \approx 120\pi$
Ω = free-space impedance
E_0 = the field of the source at a distance d on a flat perfectly conducting earth For $d/\lambda \gg 1$

$$E_0 = -i(\eta/\lambda)\ \text{Ids}\ \frac{e^{-i2\pi d/\lambda}}{d} \tag{11}$$

where

$$\delta_n = \begin{cases} \frac{1}{2}, & n = 0 \\ 1, & n = 1, 2, \ldots \end{cases}$$

$S_n = \sin\theta_n$
$\sqrt{1 - C_n^{1/2}}$ = sine of the eigenangle of the nth mode (which may be complex)
$C_n = \cos\theta_n$ cosine of the eigenangle of the nth mode
θ_n = eigenangle of the nth mode.

Equation (10) describes the field measured within the waveguide, for $a < r < a + h$. This expression is an approximation that is valid only if θ is not near 0 or π, which means that the source region and the antipode are excluded. The time dependence is $e^{j\omega t}$, where $\omega = 2\pi c/\lambda$ is the angular frequency.

As the radius of the earth a tends to infinity, the flat earth approximation [Eq. (1)] is recovered.

A first-order approximation of the effect of the earth curvature on ELF fields is obtained by multiplying the field expressions for the parallel-plate waveguide [Eqs. (1) and (4)] by the factor $1 + \theta^2/12$. The coordinate system used here is cylindrical, as in the section "Simplified Waveguide Model" above:

$$E_z = \left(1 + \frac{\theta^2}{12}\right) E_0 \frac{(\rho/\lambda)^{1/2}}{(h/\lambda)} e^{j(k\rho - \pi/4)} \sum_{n=0}^{\infty} \delta_n S_n^{3/2} e^{-jkS_n\rho} \cos(kC_n z) \qquad (12)$$

Using appropriate approximations, it can be shown that the field consists of two components. One of these components travels along the short great-circle path connecting the source and the receiver, and the other travels along the complementary long great-circle path, passing though the antipode [Wait (1)].

An interesting feature of the spherical waveguide is the antipodal concentration that causes the vertical electric field signals measured at the antipodal point to be stronger than signals measured at a similar distance away from the source in a plane parallel waveguide. This effect is caused by the addition of many coherent signal components traveling along great-circle paths between the source and the antipodal point. [The actual antipodal effect is more complex, due to the day–night terminator (see the subsection "Day–Night Terminator Effect" below) and other propagation effects in the various paths.] The antipodal concentration and other antipodal effects are discussed further in the section "Antipodal Effects" below.

Geomagnetic Field. The static geomagnetic field affects the behavior of the ionospheric boundary of the waveguide. In the presence of the geomagnetic field, the ionosphere becomes anisotropic and the ionospheric reflection coefficient depends on the angle α between the incident wavefront and the static magnetic field (see Fig. 4 for the definition of α). This adds a new dependence to the ionospheric reflection coefficient, further complicating the modal equation:

$$R_i\big(\omega, \theta_n, \alpha(\theta, \phi)\big) R_e(\omega, \theta_n) e^{-j2kh(\omega)C_n} = e^{-j2\pi n}, \qquad n = 0, 1, 2, \ldots \qquad (13)$$

The direction and intensity of the geomagnetic field depend on the geomagnetic location and, as a result, the description of the earth–ionosphere waveguide has to take this location into account.

Dinger et al. (37) show that background noise measured in Norway at frequencies near 3 kHz is not isotropic. The east–west component of the measured noise (noise propagating along an east–west or west–east path) is 1 dB to 1.5 dB lower than the north–south component during the day, but increases around local sunset to a level of about 4 dB above the north–south component. The difference between noise levels measured in the two components is explained by the anisotropy of the propagation loss, which is caused by the geomagnetic field.

Nonreciprocity of ELF Propagation. The geomagnetic field introduces a directional dependence into the attenuation of ELF waves. This is the reason why ELF waves propagating from west to east suffer higher attenuation than those propagating from east to west in middle latitudes. This difference between the properties of the propagation between east–west and west–east paths is called the nonreciprocity of the propagation.

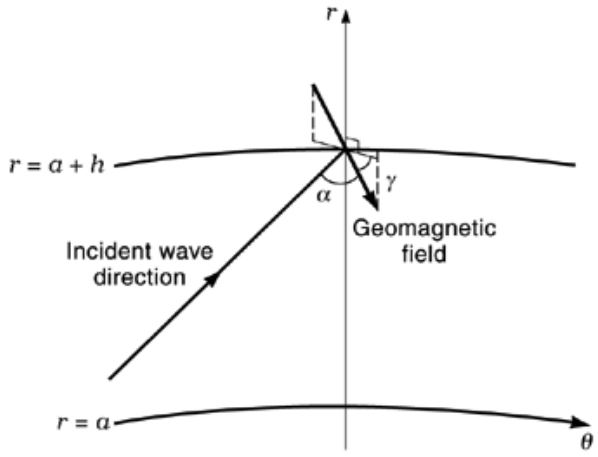

Fig. 4. Geometry of the earth–ionosphere waveguide with the geomagnetic field present. γ is the direction of the geomagnetic field relative to the horizontal. α is the angle between the incident wave direction and the geomagnetic field.

This effect is analyzed by Barr (38), who shows that the nonreciprocity is most notable for frequencies above 1 kHz. Barr (39) computes the attenuation factors for east-to-west and west-to-east propagation, and finds a difference of up to 45 dB/Mm. These results are shown to be in good agreement with measurements.

Antipodal Effects

Some fields measured at the antipodal point of a source are enhanced due to the spherical shape of the earth–ionosphere waveguide. The enhancement can be intuitively explained as the coherent addition of many waves traveling from the source to the antipodal point along great-circle paths. Galejs (14) calculates antipodal effects on the different field components generated by vertical and horizontal dipole sources. He shows that for a vertical dipole source the only field component present at the antipode is the vertical component of the electric field. For a horizontal dipole source the antipodal field contains horizontally directed electric and magnetic fields, perpendicular to each other, with the electric field parallel to the dipole axis. These results are also summarized in Ref. 40.

Wait (1) gives a brief description of antipodal effects for a vertical dipole source and shows that waves traveling through the antipode acquire a $\pi/2$ phase advance. Wait (41) and Jones (42) analyze the distortion of ELF pulses after propagation through an antipode. The $\pi/2$ phase advance of lightning-generated pulses traveling around the earth is examined.

Measurements of antipodal effects are difficult because of the long distances involved, which dictate the use of very strong sources. Measurements made on an 82 Hz signal are described in Fraser-Smith and Bannister (43). The transmitting facility was located in northwestern Russia, and measurements showing antipodal concentration were made in New Zealand and Antarctica. Similar results, in the VLF band, are reported by Rogerson (44). In this latter case the source was a U.S. Navy transmitter in Hawaii, and the measurements were taken by an aircraft in the vicinity of the antipodal point located in southern Africa.

Ionospheric Reflection

This section describes the mechanism of reflection of ELF waves from the ionosphere. The ionosphere is conductive because it contains free electrons and positive ions, which are generated largely by solar ultraviolet

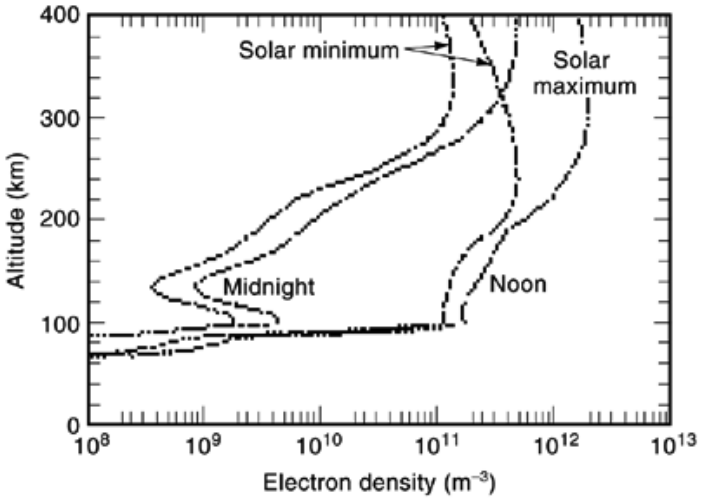

Fig. 5. Typical electron densities at 44.6°N, 2.2°E at noon and midnight on March 21, for solar minimum and maximum conditions. The electron density determines the behavior of the ionospheric wall of the earth–ionosphere waveguide. Adapted from A. D. Richmond, in H. Volland (ed.), *Handbook of Atmospheric Electrodynamics*, CRC Press, 1995, with permission (CRC Press home page http://www.crcpress.com).

(*UV*) and X radiation and by the precipitation of energetic charged particles from the magnetosphere. A discussion of the ionization generation mechanism and the various positive ions involved can be found in Richmond (45) and in other literature on the subject [Rees (46), Kato (47), Akasofu and Chapman (48), Ratcliffe (49,50), Rishbeth and Garriot (51), Whitten and Poppoff (52), and Rawer (53)].

The amount of free charge in the ionosphere is determined by the equilibrium that is reached between the generation mechanisms and the recombination of the free electrons with the positive ions. The density of neutral particles in the ionosphere decreases exponentially with increasing altitude, which means that very little generation occurs at the high altitudes (above 500 km), where the particle density is low. The energetic particles precipitating from the magnetosphere gradually lose their energy as they penetrate the ionosphere, generating free charge as they travel downward. The solar radiation penetrating the ionosphere is likewise gradually absorbed while generating free charge in the ionosphere. The bottom of the ionosphere (around 50 km) is marked by very little generation of charge, because the ionizing radiation has lost most of its energy at higher altitudes. The density of free charge in the ionosphere is maximal at middle heights, where the generating mechanisms are strong and the density of particles is sufficient. The free-electron density is maximal at an altitude of about 250 km above ground, with a few local maxima of density at lower altitudes. These local maxima constitute ionospheric layers with enhanced electron density, as seen in Fig. 5.

The layer about the altitude of 100 km is called the E layer, the layer at 170 km, which is sometimes absent at night, is the F_1 layer, and the top layer at 250 km is the F_2 or the F layer. The lowest layer, at about 70 km, is the D layer, which is almost always absent at night. A description of the structure and properties of the ionosphere is presented by Hargreaves (54).

The electron density height profile in the ionosphere differs greatly between day and night conditions, because of the different ionization generation rates driven by solar radiation. The electron density is also affected by solar activity, with the ionization being lowest during periods of low solar activity, as seen in Fig. 5.

The ionosphere is a plasma, and its conductivity can be calculated using plasma theory, as described by Rishbeth and Garriot (51), by Ratcliffe (49), and in other literature on the subject. The ionospheric plasma parameters (i.e., the types of particles and their concentrations) are altitude-dependent, so the conductivity of

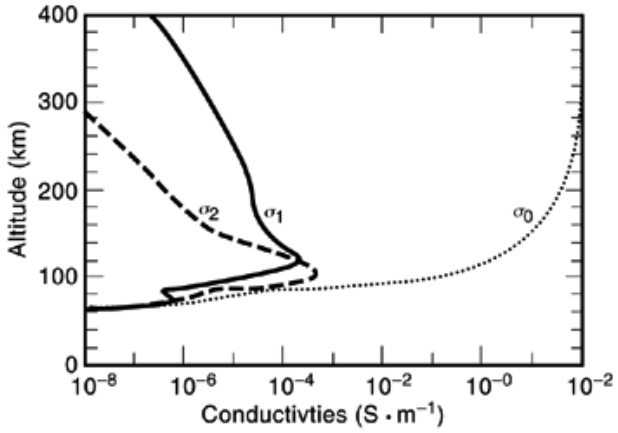

Fig. 6. Typical noontime parallel (σ_0), Pedersen (σ_1), and Hall (σ_2) conductivities at 44.6°N, 2.2°E for solar minimum conditions on March 21. The different types of conductivity characterize the behavior of the ionosphere as a reflector of ELF waves. Adapted from A. D. Richmond, in H. Volland (ed.), *Handbook of Atmospheric Electrodynamics*, CRC Press, 1995, with permission (CRC Press Home Page http://www.crcpress.com).

the ionosphere also varies with altitude. In addition, the conductivity varies in the lateral plane, with the most notable variation occurring at the day–night terminator, which marks the dawn and dusk boundaries. Local disturbances in the ionosphere also cause lateral variations of the conductivity; these variations are discussed in the section "The Inhomogeneous Ionosphere" below.

Due to the geomagnetic field, the ionosphere is an anisotropic conductor. The three most commonly used conductivities apply to specific directions relative to the geomagnetic field, as follows:

- The *Parallel conductivity* σ_0 relates the current flowing along the static magnetic field to an electric field component in the same direction. This conductivity is not affected by the presence of the static magnetic field.
- The *Pederson conductivity* σ_1 corresponds to current flowing perpendicular to the static magnetic field when an electric field is applied in the same direction.
- The *Hall conductivity* σ_2 corresponds to current flowing in a direction perpendicular to both the magnetic field and the electric field, when the electric field is perpendicular to the magnetic field.

Figure 6 shows typical midlatitude vertical profiles of the daytime conductivity components for low solar activity. At altitudes above 80 km the parallel conductivity is much larger than the Pederson and Hall conductivities.

The reflection coefficients of the ionosphere depend on (a) the conductivity profile of the ionosphere, (b) the local geomagnetic field, (c) the direction of incidence, and (d) the polarization of the incident wave. Due to the complexity of the reflection coefficients, they are usually calculated numerically or empirically. Simplified empirical expressions for the reflection coefficients in day and night conditions are given in Volland (55) for a simplified model characterized by an exponential electron density and an exponential collision rate in the lower layers of the ionosphere. The effects of the geomagnetic field are neglected. The reflection coefficient for TM waves under these simplified conditions is

$$R_{\mathrm{i}} \approx e^{-(b_{\mathrm{i}} - jc_{\mathrm{i}})/\cos\theta} \tag{14}$$

where b_{i} and c_{i} vary exponentially with frequency and θ is the incidence angle.

Harth (34) calculates the ionospheric reflection coefficient at 3 kHz using a thin-layer method (see the final section for a discussion of the thin-layer method) with similar assumptions to Volland's, and the results are presented graphically. Wait and Spies (56) present graphs describing the reflection coefficient for an exponential electron density profile under various conditions. They show the effects of the magnetic field, angle of incidence, frequency, reflecting height, and ground conductivity on the reflection coefficient. An experiment relating electron density profiles to VLF reflection coefficients is described by Mambo et al. (57).

A different approach to the calculation of the reflection coefficients is taken by Budden (58), who presents a plasma physics approach to understanding the ionosphere. The calculation of the refractive index and the characteristic polarization of waves traveling through the ionosphere is the basis of this approach. The admittance matrix of the ionosphere is calculated, which relates the horizontal components of the electric and magnetic field, and the reflection coefficients of the ionosphere are then derived from the matrix expressions. Two types of ionospheric boundaries are considered: a sharp boundary and a slowly varying one [Wentzel–Kramers–Brillouin (WKB) model]. A similar approach is taken by Galejs (14), where the modal equations are presented in terms of the wave impedance rather than the reflection coefficient.

The ionosphere can usually be modeled as a sharp boundary for frequencies in the ELF range, since the wavelengths are large compared to the scales of length over which the ionospheric properties change. As a result, a simplified model of the ionosphere with a sharp bottom boundary is often sufficient.

The Inhomogeneous Ionosphere

A realistic picture of ELF propagation in the earth–ionosphere waveguide has to take into account the effects of inhomogeneities in the ionosphere. The vertical structure of the ionosphere, as represented by the ionospheric layers, was described in the subsection "Reflection Coefficients." The following section describes the effects of the lateral structures and variations in the ionosphere on ELF propagation.

The lateral structure of the ionosphere and various inhomogeneities affect the propagation loss in the ELF range, and some affect the propagation path. However, compared to other frequency bands, propagation in the ELF band appears more stable under ionospheric disturbances.

Day–Night Terminator Effect. The line marking the transition between day and night is called the day–night terminator, or simply the terminator, and the transition has a profound effect on propagating ELF radiation. Measurements show that the phase velocity of ELF waves traveling across the day–night terminator can be approximated as a weighted average of day and night phase velocities, with each velocity given a weight according to the length of the path in the two regions [Hughes and Gallenberger (59)]. The loss in mixed day–night paths varies in a more complex manner with the percentage of the sunlit section in the path. Measurements at 400 Hz show deep fades when the day–night terminator is located above the receiver [Davis (60)], which are not explained by a smooth transition between day and night regions.

ELF waves are also reflected from the day–night terminator. Bezrodnyi et al. (61) measure a reflection coefficient for VLF signals using the Doppler shift produced by the terminator motion. Their measurements show that the reflection coefficient is on the order of 10^{-2} to 10^{-3}. Field and Joiner (62) calculate the lateral refection and transmission coefficients of ELF TEM waves from the terminator.

Theoretical analysis of the effects of the terminator on ELF propagation is given by Nikolaenko (63) and by Field and Joiner (62). Nikolaenko (63) calculates the effect of the terminator in three geometrical arrangements, describing different directions of wave propagation relative to the terminator (parallel, perpendicular, and inclined). Figure 7 shows the perturbation in the vertical electric field from the homogeneous ionosphere model for an inclined propagation path relative to the terminator.

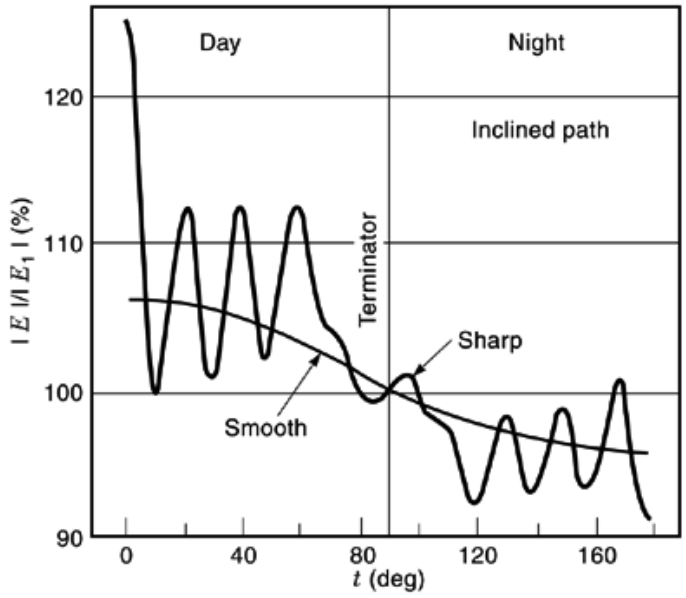

Fig. 7. Amplitude of the vertical electric field in a propagation path inclined 45° from the terminator, relative to the unperturbed field in the models of the smooth and sharp terminators. The day night terminator is the main source of lateral variation in the earth–ionosphere waveguide. Adapted from A. P. Nikolaenko, in *Radiophysics and Quantum Electronics*, Vol. 29, No. 1, Plenum Publishing Corporation, 1986, with permission.

Ionospheric Disturbances.

Varieties of Disturbances. Three major varieties of ionospheric disturbances are: (1) sudden ionospheric disturbances (*SID*s), (2) magnetic storms, and (3) solar proton events (*SPE*s), also called proton storms (51). They can be defined as follows:

- *Sudden ionospheric disturbances* are related to *solar flares*, electromagnetic phenomena that enhance the electron density of the D region by up to a factor of ten.
- *Magnetic storms* are caused by enhancements of the *solar wind*, a stream of particles traveling away from the sun. An increase in the particle concentration of the solar wind, accompanied by an increase in their velocity, causes ionospheric modifications where it reaches the magnetosphere, which result in magnetic storms. The solar wind enhancements are usually associated with the solar events known as coronal mass ejections or CME's.
- *Solar proton events* are caused by energetic streams of solar protons (accompanied by electrons). On arrival at the earth the protons are deviated by the geomagnetic field, and they impinge on the polar caps, so solar proton events are related to polar cap absorption (*PCA*) events.

Other ionospheric disturbances include the effect of sporadic E layers and small-scale ionospheric irregularities. A summary of ionospheric disturbances and their effect on radio propagation is given by Hargreaves (54).

General Considerations. The theoretical analysis of ionospheric inhomogeneities often involves calculations of the electromagnetic field scattered from the inhomogeneities. Pappert (64) calculates the field scattered from a cylindrically symmetric ionospheric disturbance and compares the expected effect of disturbed polar-cap

boundaries with measurements. The cylindrically symmetric ionospheric disturbance model is also useful in describing small-scale ionospheric irregularities.

The effect of local ionospheric disturbances on ELF propagation is analyzed by Nickolaenko (65,66) using a perturbation theory. The disturbances analyzed are (1) local variations of the electrical properties of the ionosphere and (2) changes in the effective ionospheric reflection height. The analysis shows that the effects of these two types of disturbances on ELF propagation are similar and that the effect of local disturbances is greatest when the irregularity is situated above the source or the observer.

Random distortions in ionospheric height and fluctuations of electrical properties cause fluctuations of ELF waves propagating in the earth–ionosphere waveguide; these are analyzed by Kostigov (67) using a perturbation method.

Specific Effects. Ionospheric inhomogeneous phenomena affect ELF waves traveling between the ionosphere and the earth. Bannister (4) reviews measurements of various ELF propagation phenomena related to ionospheric irregularities, some of which are mentioned below.

The effects of sudden ionospheric disturbances caused by solar flares on ELF propagation are analyzed by Field (68), and the resulting modal attenuation coefficients are compared with measurements. The X-ray radiation associated with solar flares causes a lowering of the D layer, which reduces the propagation loss in the ELF range relative to nondisturbed conditions.

Precipitation of energetic electrons in the several days following magnetic storms may cause enhanced loss in the ELF range at night. Measurements showing this effect are described by Davis (69) and Bannister (4), but the theoretical explanation is incomplete. Three different groups analyzed a magnetic storm that occurred in December 1971 using satellite measurements, and all of them measured enhanced electron precipitation and enhanced levels of ELF radiation [Parady and Cahill (70), Vakulov et al. (71), and Kovner et al. (72)]. These results suggest that the relationship between the electron precipitation and the ELF fields is connected with the location of the magnetopause, that is, the outer termination of the geomagnetic field.

Occasional nighttime decreases in ELF signal levels may be explained by the presence of sporadic E layers [Bannister (4,73)]. The measurements described by Bannister include ELF anomalies at two different locations, appearing 2 h to 4 h apart, which may be the result of a traveling sporadic E layer. Further analysis of the measurements from these two locations yields an estimate of the velocity and path of the sporadic E layer [Pappert (74)].

Theoretical analyses of the effect of sporadic E layers on ELF propagation are given by Pappert (75) and by Pappert and Moler (76). Their results indicate that a sporadic E layer 1 Mm by 1 Mm may cause 6 dB to 8 dB attenuation in the ELF range. Patches 1 Mm by 0.5 Mm can account for fades in the 3 dB to 4 dB range. The deepest fades require the center of the disturbance to be close either to the source or to the receiver, but large patches cause significant attenuation at distances of up to 10 Mm from the direct propagation path between the source and receiver.

The main effect of a SPE is an increase in the attenuation in the ELF range for paths passing near the boundary of the polar cap [Katan and Bannister (77), Field et al. (78) and Fraser-Smith and Helliwell (79)]. The additional attenuation may be caused by lateral refraction, which bends the signal path away from the polar-cap boundary and into the central cap zone. Field et al. (78) predict enhanced field levels inside the polar-cap boundary, but this was not verified by measurement.

The expected effects of nuclear events on ELF propagation via ionospheric changes is surveyed by Bannister (4).

ELF Calculation Methods

This section describes the approaches used to calculate ELF fields in the earth–ionosphere waveguide. As already indicated, an accurate representation of the earth–ionosphere waveguide is extremely complex, and

calculations are often done numerically, incorporating information about various ionospheric and ground parameters.

The two main computational approaches presented here, namely (a) the full-wave approach and (b) the thin-layer approach, are suitable for a horizontally stratified ionosphere with no lateral variation. Calculation methods for laterally varying ionospheres are also surveyed.

A noniterative approximate method for calculating eigenvalues of the ELF modes, based on a two-layer ionospheric model, is presented by Greifinger and Greifinger (36) and elaborated by them in Ref. 80. The physical significance of a reflecting layer for ELF waves within the ionosphere is discussed in those papers.

The Full-Wave Approach. The full-wave approach involves the numerical integration of four coupled first-order complex differential equations containing an eigenvalue parameter [Greifinger and Greifinger (80)]. The calculated quantities may be (a) the components of the electromagnetic field, (b) ratios of field components, which may represent impedances, and (c) reflection coefficients. The full-wave integration starts from the top of the ionosphere, where propagation is assumed to be upward only. An initial value of propagation parameters is assumed at this height. Integration is performed downward along a vertical path, and boundary conditions are checked at the surface of the earth. Inconsistencies of the boundary conditions at the surface of the earth lead to corrections of the initial value (of propagation parameters at the top of the ionosphere), and the whole process repeats with new initial values, until the boundary conditions are matched to some chosen accuracy.

A full-wave calculation of the ionospheric reflection coefficients is described by Pappert and Moler (81). The ionosphere is assumed to vary slowly along the lateral propagation path, and the WKB approximation is used.

Field (82) uses a full-wave method to calculate the ionospheric wave admittance for normal and disturbed ionospheric conditions, and calculates the fields within the waveguide.

Aksenov and Nazarova (83) use a full-wave method to calculate the dependence of ionospheric reflection and transmission coefficients on the angle of incidence, frequency, and geomagnetic field for ionospheric models of the day and night.

The Thin-Layer Approach. The thin-layer approach is similar in principle to the full-wave approach, but the ionosphere is taken to be a collection of thin homogeneous layers, rather then a continuum. The process is started with some initial values of the parameters at the top boundary of the ionosphere, and then the boundary conditions are matched between adjacent layers, going downward until a lower boundary is reached. The thin-layer method is iterative in a similar way to the full-wave method: the boundary conditions at the lower boundary are used to correct the initial values, and the calculation process is repeated until convergence is achieved to a desired accuracy.

Galejs (84) presents a thin-layer method where the surface impedance computed at a lower boundary is used to correct the initial conditions. The field components are calculated for each layer, and from these the wave impedances are derived. This procedure is used to calculate the frequency-dependent attenuation rate for day and night conditions and to examine the effect of the anisotropy of the ionosphere.

A similar approach is presented by Altman and Cory (85,86), where the ionosphere is treated as a collection of discrete layers and an iterative process is used to calculate ELF propagation parameters, each iteration starting from the top of the ionosphere. This method is presented as a derivation from the thin-film method used in optics.

Another thin-layer method is presented by Nagano et al. (87), where the calculated quantities are the components of the field. Nagano et al. (87) compare the width of the layers required for their method with the step size required in various full-wave methods and show that their thin-layer method produces comparable results to full-wave methods, with much bigger step sizes. The complexity (computer time) of the two methods is also compared, and it is shown that the thin-layer method is more efficient.

Lateral Variations in the Waveguide. Lateral variations in the earth–ionosphere waveguide may be treated by the WKB approach, which assumes slow variation in the waveguide. However, this approach is of

little use in the ELF band, because the wavelengths involved are very large, with the result that in many cases the ionospheric or ground variations are not slow compared to the wavelength.

An important approach to lateral variations in the waveguide is based on an integral equation describing the lateral propagation [Field and Joiner (88)]. The integral equation is solved numerically in terms of the sine of the eigenangle. This approach is based on the simplified assumptions that vertical variations in the ionosphere are decoupled from lateral variations and that lateral variations are much slower than vertical variations. A program that predicts vertical ELF fields in an inhomogeneous waveguide is described by Ferguson et al. (89). This program uses the moment method to solve the integral equation numerically.

Another approach to the laterally varying waveguide is based on ray theory, where vertical inhomogeneities are assumed to be uncoupled from the lateral variations. The vertical inhomogeneities are usually treated in a full-wave approach, and the lateral variations are treated using ray theory. Field et al. (78) use the full-wave–ray method to analyze the effects of polar-cap absorption events on ELF propagation.

A calculation of the electric field, given the eigenvalues of the propagation, is described by Shellman (90). The method is based on the knowledge of the sine of the waveguide eigenangles at elements of a mesh-point array that extends around the earth. The lateral variation of the waveguide is described by the eigenvalues at different locations.

Acknowledgments

The authors thank Martin Füllekrug for the Schumann resonance data plotted in Fig. 2.

This work was supported in part by the Office of Naval Research through Grant N00014-92-J-1576.

BIBLIOGRAPHY

1. J. R. Wait *Electromagnetic Waves in Stratified Media*, revised ed. 1970. New York: Pergamon Press.
2. P. R. Bannister Simplified formulas for ELF propagation at shorter distances *, Radio Sci.* **21** (3): 529–537, 1986.
3. A. P. Nickolaenko M. Hayakawa Natural electromagnetic pulses in the ELF range *, Geophys. Res. Lett.* **25** (16): 3103–3106, 1998.
4. P. R. Bannister ELF propagation update *, IEEE J. Oceanic Eng.* **OE-9**: 179–188, 1984.
5. F. J. Kelly ELF/VLF/LF propagation and system design, Technical Report NRL 9028, Naval Research Laboratory, June 1987.
6. J. Villaseñnor *et al.* Comparison of ELF/VLF generation modes in the ionosphere by the HIPAS heater array *, Radio Sci.*, **31** (1): 211–226, 1996.
7. R. Barr P. Stubbe. ELF and VLF radiation from the "polar electrojet antenna," *Radio Sci.*, **19** (4): 1111–1122, 1984.
8. K. Papadopoulos *et al.* On the efficiency of ionospheric ELF generation, *Radio Sci.*, **25** (6): 1311–1320, 1990.
9. P. Stubbe *et al.* Ionospheric modification experiments with the TromsØ Heating Facility, *J. Atm. Terrestrial Phys.*, **47** (12): 1151–1163, 1985.
10. A. J. Ferraro *et al.* Measurements of extremely low frequency signals from modulation of the polar electrojet above Fairbanks, Alaska, *IEEE Trans. Antennas Propag.*, **37**: 802–805, 1989.
11. R. Barr *et al.* ELF and VLF signals radiated by the "polar electrojet antenna": Experimental results, *J. Geophys. Res.*, **91** (A4): 4451–4459, 1986.
12. M. T. Rietveld *et al.* Ionospheric heater beam scanning: A new technique for ELF studies of the auroral ionosphere, *Radio Sci.*, **19** (4): 1069–1077, 1984.
13. R. Barr *et al.* Ionospheric heater bean scanning: A mobile source of ELF radiation. *Radio Sci.*, **22** (6): 1073–1083, 1987.
14. J. Galejs *Terrestrial Propagation of Long Electromagnetic Waves*, New York: Pergamon, 1972.
15. E. L. Maxwell Atmospheric noise from 20 Hz to 30 kHz, *Radio Sci.*, **2** (6): 637–644, 1967.

16. E. L. Maxwell D. L. Stone Natural noise fields from 1 cps to 100 kc, *IEEE Trans. Antennas Propag.* **AP-11** (3): 339–343, 1963.
17. G. Gustafsson A. Egeland J. Aarons Audio-frequency electromagnetic radiation in the auroral zone, *J. Geophys. Res.* **65** (9): 2749–2758, 1960.
18. A. J. Smith P. J. Jenkins A survey of natural electromagnetic noise in the frequency range $f = 1$–10 kHz at Halley station, Antarctica: 1. Radio atmospherics from lightning, *J. Atm. Solar–Terrestrial Phys.*, **60** (2): 263–277, 1998.
19. J. R. Wait Earth–ionosphere cavity resonances and the propagation of ELF radio waves, *Radio Sci.*, **69D** (8): 1057–1070, 1965.
20. D. L. Jones Numerical computations of terrestrial ELF electromagnetic wave fields in the frequency domain, *Radio Sci.* **5** (5): 803–809, 1970.
21. D. B. Large J. R. Wait Theory of electromagnetic coupling phenomena in the earth–ionosphere cavity, *J. Geophys. Res.* **73** (13): 4335–4362, 1968.
22. M. Balser C. A. Wagner Observations of earth–ionosphere cavity resonances, *Nature*, **188**: 638–641, 1960.
23. M. Balser C. A. Wagner Diurnal power variations of the earth–ionosphere cavity modes and their relationship to worldwide thunderstorm activity, *J. Geophys. Res.* **67** (2): 619–625, 1962.
24. A. P. Nickolaenko L. M. Rabinowicz Study of the annual changes of global lightning distribution and frequency variations of the first Schumann resonance mode, *J. Atm. Terrestrial Phys.* **57** (11): 1345–1348, 1995.
25. A. P. Nickolaenko M. Hayakawa Y. Hobara Temporal variations of the global lightning activity deduced from the Schumann resonance data, *J. Atm. Terrestrial Phys.* **58** (15): 1699–1709, 1996.
26. T. Ogawa Y. Tanaka M. Yasuhara Schumann resonances and worldwide thunderstorm activity, in S. C. Coroniti and J. Hughes, (ed.), *Planetary Electrodynamics*, Vol. 2, New York: Gordon and Breach, 1969, Chap. V-7.
27. S. J. Heckman E. Williams B. Boldi Total global lightning inferred from Schumann resonance measurements, *J. Geophys. Res.* **103** (D24): 31, 775–31, 779, 1998.
28. C. Polk Relation of ELF noise and Schumann resonances to thunderstorm activity, in S. C. Coroniti and J. Hughes (ed.), *Planetary Electrodynamics*, Vol. 2, New York: Gordon and Breach 1969, chap. V-6. pp. 58–63.
29. J. Galejs Frequency variations of Schumann resonances, *J. Geophys. Res.* **75** (16): 3237–3251, 1970.
30. D. D. Sentman B. J. Fraser Simultaneous observations of Schumann resonances in California and Australia: Evidence for intensity modulation by the local height of the D region, *J. Geophys. Res.* **96** (A9): 15,973–15,984, 1991.
31. K. Sao *et al.* Experimental investigations of Schumann resonance frequencies, *J. Atm. Terrestrial Phys.* **35**: 2047–2053, 1973.
32. E. R. Williams The Schumann resonance: A global tropical thermometer, *Science* **256**: 1184–1187, 1992.
33. A. P. Nickolaenko Modern aspects of Schumann resonance studies, *J. Atm. Solar–Terrestrial Phys.*, **59** (7): 805–816, 1997.
34. W. Harth Theory of low frequency wave propagation, in H. Volland (ed.), *CRC Handbook of Atmospherics*, Vol. II, CRC Press, Boca Raton, FL, 1982, pp. 133–202.
35. H. G. Booker F. Lefeuvre The relation between ionospheric profiles and ELF propagation in the earth–ionosphere transmission line, *J. Atm. Terrestrial Phys.*, **39**: 1277–1292, 1977.
36. C. Greifinger P. Greifinger Approximate method for determining ELF eigenvalues in the earth–ionosphere waveguide, *Radio Sci.*, **13** (5): 831–837, 1978.
37. R. J. Dinger W. D. Meyers J. R. Davis Experimental investigation of ambient electromagnetic noise from 1.0 to 4.0 kHz in Italy and Norway, *Radio Sci.*, **17** (1): 285–302, 1982.
38. R. Barr Some new features of ELF attenuation, *J. Atm. Terrestrial Phys.* **34**: 411–420, 1972.
39. R. Barr The propagation of ELF and VLF radio waves beneath an inhomogeneous anisotropic ionosphere, *J. Atm. Terrestrial Phys.* **33**: 343–353, 1971.
40. J. Galejs Near fields and antipodal fields in the terrestrial earth–ionosphere waveguide, *Proc. IEE* **116** (7): 1150–1158, 1969.
41. J. R. Wait Distortion of an ELF pulses after propagation through an antipode, *J. Geophys. Res.* **74** (11):2982–2986, 1969.
42. D. L. Jones Propagation of ELF pulses in the earth–ionosphere cavity and application to "slow tail" atmospherics, *Radio Sci.* **5** (8,9): 1153–1162, 1970.
43. A. C. Fraser-Smith P. R. Bannister Reception of ELF signals at antipodal distances, *Radio Sci.* **33** (1): 83–88, 1998.
44. J. E. Rogerson Airborne field strength measurements in the region of the NPM antipode, *Radio Sci.* **2** (6): 581–587, 1967.

45. A. D. Richmond The ionospheric wind dynamo: Effects of its coupling with different atmospheric regions, in R. M. Johnson and T. L. Killeen (eds.), *The Upper Mesosphere and Lower Thermosphere*, Washington: American Geophysical Union, 1995.
46. M. H. Rees. *Physics and Chemistry of the Upper Atmosphere*, Cambridge University Press, 1989.
47. S. Kato *Dynamics of the Upper Atmosphere*, Dordrecht: Reidel, 1980.
48. S. I. Akasofu S. Chapman *Solar–Terrestrial Physics*, Oxford: Clarendon, 1972.
49. J. A. Ratcliffe *An Introduction to the Ionosphere and Magnetosphere*, Cambridge University Press, 1972.
50. J. A. Ratcliffe *Sun, Earth and Radio*, McGraw-Hill, 1970.
51. H. Rishbeth O. K. Garriot *Introduction to Ionospheric Physics*, Academic Press, 1969.
52. R. C. Whitten I. G. Poppoff *Physics of the Lower Ionosphere*, Engelwood Cliffs, NJ: Prentice-Hall, 1965.
53. K. Rawer *The Ionosphere: Its Significance for Geophysics and Radio Communications*, New York: Ungar, 1957.
54. J. K. Hargreaves *The Solar–Terrestrial Environment*, Cambridge Atmospheric and Space Science Series, Cambridge University Press, 1992.
55. H. Volland Longwave sferics propagation within the atmospheric waveguide, in H. Volland (ed.), *Handbook of Atmospheric Electrodynamics*, Vol. II, Boca Raton, FL: CRC Press, 1995, Chap. 3, pp. 65–93.
56. J. R. Wait K. P. Spies Characteristics of the earth–ionosphere waveguide for VLF radio waves, Technical Note 300, National Bureau of Standards, 1964.
57. M. Mambo, *et al.* An improved method of estimating electron density profiles in the lower ionosphere with VLF reflection coefficients, *Electron. Commun. Japan*, **67-B** (7): 28–37, 1984.
58. K. G. Budden *The Propagation of Radio Waves*, Cambridge University Press, 1985.
59. H. G. Hughes R. J. Gallenberger Propagation of extremely low-frequency (ELF) atmospherics over a mixed day–night path, *J. Atm. Terrestrial Phys.* **36**: 1643–1661, 1974.
60. J. R. Davis ELF propagation irregularities on northern and mid-latitude paths, in J. A. Holtet, (ed.), ELF–VLF Radio Wave Propagation Proc. NATO Advanced Study Institute, April 17–27, 1974, Dordrecht: D. Reidel, 1974, pp. 263–277.
61. V. G. Bezrodnyi *et al.* Reflection of superlong waves from the terminator in the earth–ionosphere waveguide, *Radiophys. Quantum Electron.*, **21** (11): 1100–1114, 1978.
62. E. C. Field R. G. Joiner Effects of lateral ionospheric gradients on ELF propagation, *Radio Sci.*, **17** (3): 693–700, 1982.
63. A. P. Nikolaenko Scattering of ELF radio waves on global inhomogeneities of the earth–ionosphere cavity, *Radiophys. Quantum Electron.*, **29** (1): 26–32, 1986.
64. R. A. Pappert ELF scattering in the earth–ionosphere waveguide, *Radio Sci.*, **24** (5): 629–639, 1989.
65. A. P. Nickolaenko ELF radio wave propagation in a locally nonuniform earth–ionosphere cavity, *Radio Sci.*, **29** (5): 1187–1199, 1994.
66. A. P. Nikolaenko Effects of a local inhomogeneity in the ionosphere on the propagation of ELF radio waves, *Radiophys. Quantum Electron.*, **27** (10): 856–864, 1984.
67. K. I. Kostigov Theory of fluctuations of super-long radio waves caused by random deformations of the boundaries of the earth surface—ionosphere waveguide channel, *Radio Eng. Electron. Phys.*, **19** (8): 123–126, 1974.
68. E. C. Field VLF and ELF propagation during sudden ionospheric disturbances, *J. Geophys. Res.*, **75** (10): 927–933, 1970.
69. J. R. Davis Localized nighttime D-region disturbances and ELF propagation, *J. Atm. Terrestrial Phys.*, **38**: 1309–1317, 1976.
70. B. Parady L. J. Cahill, Jr. ELF observations during the December 1971 storm, *J. Geophys. Res.*, **78** (22): 4765–4770, 1973.
71. P. V. Vakulov *et al.* Spilling of charged particles from the radiation belts and variations in the intensity of the ELF radiation in the recovery phase of the magnetic storm of December 16–17, 1971, *Cosmic Res.*, **12** (5): 645–652, 1974.
72. M. S. Kovner *et al.* High-energy electron flux and ELF radiation flux at ionospheric heights during the magnetic storm of December 16, 1971, *Cosmic Res.*, **15** (3): 374–379, 1977.
73. P. R. Bannister Localized ELF nocturnal propagation anomalies, *Radio Sci.*, **17** (3): 627–634, 1982.
74. R. A. Pappert Calculated effects of traveling sporadic E on nocturnal ELF propagation: Comparison with measurement, *Radio Sci.*, **20** (2): 229–246, 1985.
75. R. A. Pappert Effects of a large patch of sporadic-E on night-time propagation at lower ELF, *J. Atm. Terrestrial Phys.*, **42**, 417–425, 1980.
76. R. A. Pappert W. F. Moler A theoretical study of ELF normal mode reflection and absorption produced by night-time ionospheres, *J. Atm. Terrestrial Phys.*, **40**: 1031–1045, 1978.

77. J. R. Katan P. R. Bannister Summary of ELF propagation variations at mid and high latitudes during the November/December 1982 and February 1984 solar proton events, *Radio Sci.*, **22** (1): 111–124, 1987.
78. E. C. Field C. R. Warber R. G. Joiner Effects of the ionosphere on ELF signals during polar cap absorption event: Comparison of theory and experiments, in H. Soicher, (ed.), AGARD Conf. Proc. No. 382: Propagation Effects on Military Systems in the High Latitude Region, North Atlantic Treaty Organization, 1985, 8.3-1-8.3-10.
79. A. C. Fraser-Smith R. A. Helliwell ELF sferic occurrences in the antarctic during a solar proton event: Case study of occurrences at Byrd station during the event of June 9, 1968, *J. Geophys. Res.*, **85** (A5): 2296–2306, 1980.
80. C. Greifinger P. S. Greifinger Noniterative procedure for calculating ELF mode constants in the anisotropic earth–ionosphere waveguide, *Radio Sci.*, **21** (6): 981–990, 1986.
81. R. A. Pappert W. F. Moler Propagation theory and calculations at lower extremely low frequencies (ELF), *IEEE Trans. Commun.*, **COM-22** (4): 438–451, 1974.
82. E. C. Field Propagation of ELF waves under normal and naturally disturbed conditions, *J. Geophys. Res.*, **74** (14): 3639–3650, 1969.
83. V. I. Aksenov M. V. Nazarova Numerical solution of the problem of transmission of ELF waves through the lower ionosphere, *Radio Eng. Electron. Phys.*, **17** (7): 1057–1064, 1972.
84. J. Galejs On the terrestrial propagation of ELF and VLF waves in the presence of a radial magnetic field, *Radio Sci. J. Res. NBS/USNC-URSI*, **69D** (5): 705–720, 1965.
85. C. Altman H. Cory The simple thin-film optical method in electromagnetic wave propagation, *Radio Sci.*, **4** (5): 449–457, 1969.
86. C. Altman H. Cory The generalized thin-film optical method in electromagnetic wave propagation, *Radio Sci.*, **4** (5): 459–470, 1969.
87. I. Nagano M. Mambo G. Hutatsuishi Numerical calculation of electromagnetic waves in an anisotropic multilayered medium, *Radio Sci.*, **10** (6): 611–617, 1975.
88. E. C. Field R. G. Joiner An integral-equation approach to long-wave propagation in a nonstratified earth–ionosphere waveguide, *Radio Sci.*, **14** (6): 1057–1068, 1979.
89. J. A. Ferguson L. R. Hitney R. A. Pappert A program to compute vertical electric ELF fields in a laterally inhomogeneous earth–ionosphere waveguide, Technical Report NOCS TR 851, Naval Ocean Systems Center, San Diego, CA, 1982.
90. C. H. Shellman A model for propagation of ELF waves throughout the lateral extent of the inhomogeneous earth–ionosphere waveguide, *Radio Sci.*, **24** (1): 35–46, 1989.

DANA PORRAT
ANTONY C. FRASER-SMITH
Stanford University